Homeostatic scaling of neuronal excitability by synaptic modulation of somatic hyperpolarization-activated I_h channels

Ingrid van Welie*, Johannes A. van Hooft, and Wytse J. Wadman

Section of Neurobiology, Swammerdam Institute for Life Sciences, University of Amsterdam, P.O. Box 94084, NL-1090 GB, Amsterdam, The Netherlands

Edited by Charles F. Stevens, The Salk Institute for Biological Studies, La Jolla, CA, and approved February 23, 2004 (received for review November 20, 2003)

The hyperpolarization-activated cation current (I_h) plays an important role in determining membrane potential and firing characteristics of neurons and therefore is a potential target for regulation of intrinsic excitability. Here we show that an increase in AMPA-receptor-dependent synaptic activity induced by α-latrotoxin or glutamate application as well as direct depolarization results in an increase in I_h recorded from cell-attached patches in hippocampal CA1 pyramidal neurons. This mechanism requires Ca^{2+} influx but not increased levels of cAMP. Artificially increasing I_h by using a dynamic clamp during whole-cell current clamp recordings results in reduced firing rates in response to depolarizing current injections. We conclude that modulation of somatic I_h represents a previously uncharacterized mechanism of homeostatic plasticity, allowing a neuron to control its excitability in response to changes in synaptic activity on a relatively short-term time scale.

The intrinsic excitability of neurons determines the translation from synaptic input to axonal output. Regulation of intrinsic excitability may therefore constitute a form of cellular plasticity that controls the dynamic range of the input–output relationship. Such a mechanism of cellular plasticity may exist in parallel to synapse-specific mechanisms of plasticity like long-term potentiation and long-term depression. There is increasing evidence for the existence of mechanisms of plasticity that are not synapse-specific but act at the cellular level (1–3). Long-lasting changes in synaptic activity over several days have been shown to modulate the intrinsic voltage-gated ionic conductances that shape neuronal firing patterns (4–6). Modulation of voltage-gated conductances occurring at a time scale of hours has also been reported (7, 8). However, under physiological conditions, where the level of synaptic activity can change quickly, modulation of somatic voltage-gated conductances may be a potent mechanism to regulate excitability. It is unknown, however, whether such a mechanism of plasticity exists on a relatively short-term time scale.

Hyperpolarization-activated cation channels (I_h) are a subset of voltage-gated channels that are important in determining intrinsic excitability. I_h channels, which are permeable to both Na^+ and K^+ ions, operate in the subthreshold voltage range where they influence membrane potential, firing threshold, and firing patterns, as well as synaptic integration (9–14). Here we show that somatic I_h channels in rat hippocampal CA1 pyramidal neurons are subject to modulation by an enhancement of synaptic activity on a time scale of tens of minutes and that this modulation reduces the excitability of these neurons.

Methods

Slice Preparation and Electrophysiology. Parasaggital hippocampal slices (250 μm) were prepared from 14- to 28-day-old male Wistar rats (Harlan, Zeist, The Netherlands). Experiments were conducted according to the ethics committee guidelines for animal experimentation of the University of Amsterdam. After decapitation, the brain was rapidly removed and placed in ice-cold artificial cerebrospinal fluid (ACSF) containing 120 mM NaCl, 3.5 mM KCl, 2.5 mM $CaCl_2$, 1.3 mM $MgSO_4$, 1.25 mM NaH_2PO_4, 25 mM glucose, and 25 mM $NaHCO_3$, equilibrated with 95% O_2 and 5% CO_2 (pH 7.4). Subsequently, slices were cut by using a vibroslicer (752 M, Campden Instruments, Loughborough, U.K.) and allowed to recover for 1 h at 31°C. CA1 pyramidal neurons were visualized with an upright Zeiss Axioskop with Hoffman modulation contrast optics and a VX44 charge-coupled device camera (PCO, Kelheim, Germany). During voltage clamp experiments, slices were continuously superfused with ACSF supplemented with 1 μM tetrodotoxin (Latoxan, Valence, France). Patch clamp recordings were made at room temperature.

For whole-cell voltage and current clamp experiments, patch pipettes were pulled from borosilicate glass and had a resistance of 2–4 MΩ when filled with 140 mM potassium gluconate, 10 mM Hepes, 5 mM EGTA, 0.5 mM $CaCl_2$, 2 mM Mg-ATP, and 10 mM sucrose (pH 7.4 with KOH). In whole-cell voltage clamp experiments, I_h channels in the somatic compartment (defined as the soma together with the basal dendrites and the initial segment of the apical dendrite) were isolated from the majority of dendritic I_h channels by placing a cut in stratum radiatum parallel to the CA1 pyramidal cell layer, under the visual guidance of a dissecting microscope. The distance of the cut from the pyramidal cell layer was determined once slices were placed into the recording chamber and ranged from 80 to 120 μm. Currents were activated by hyperpolarizing voltage steps (1,000 ms) from a holding potential of −50 mV. Series resistance was compensated for 80%. Current signals in voltage clamp were filtered at 333 Hz and sampled at 1 kHz by using an EPC9 amplifier and PULSE 8.31 software (HEKA Electronik, Lambrecht, Germany). Voltage signals in current clamp were filtered at 3.33 kHz and sampled at 10 kHz.

For experiments in the cell-attached configuration, patch pipettes were pulled from borosilicate glass and had a resistance of 1.5–3 MΩ when filled with 120 mM NaCl, 10 mM Hepes, 3 mM KCl, 1 mM $MgCl_2$, and 1 μM tetrodotoxin (pH 7.4 with NaOH). Note that in the cell-attached configuration, the pipette potential and the resting membrane potential are positioned in series to form the local transmembrane potential over the patch, i.e., a pipette potential of 0 mV refers to the resting membrane potential. In this recording configuration, applying a positive pipette potential results in membrane hyperpolarization, and applying a negative pipette potential results in membrane depolarization, exactly opposite to sign conventions in the whole-cell configuration. In the text and figures, we give membrane potentials relative to the resting membrane potential, but we use the standard sign convention that negative potentials indicate a hyperpolarization and positive potentials indicate a depolariza-

This paper was submitted directly (Track II) to the PNAS office.

Abbreviations: I_h, hyperpolarization-activated cation current; α-LTX, α-latrotoxin; ACSF, artificial cerebrospinal fluid; CNQX, 6-cyano-7-nitroquinoxaline-2,3-dione disodium; GABA, γ-aminobutyric acid; $[Ca^{2+}]_i$, intracellular Ca^{2+} concentration.

*To whom correspondence should be addressed. E-mail: welie@science.uva.nl.

tion. Currents were evoked by hyperpolarizing voltage steps (1,000 ms) from a relative membrane potential of +20 mV.

To enhance synaptic activity, α-latrotoxin (α-LTX; dissolved in 50% glycerol, final concentration 0.15 nM in ACSF) was bath-applied for 15–25 min (15). The enhancement of synaptic activity by α-LTX was confirmed by separate experiments in which miniature synaptic events were recorded in whole-cell voltage clamp mode. Glutamate (100 μM), γ-aminobutyric acid (GABA) (100 μM), ACSF, or KCl (50 mM) were locally applied from a second pipette connected to a picospritzer (General Valve, Fairfield, NJ) by short and repeated pressure applications of 100 ms for 4 s at 5 Hz at 10-s intervals. Hyperpolarization-activated currents were recorded in the 10-s intervals.

To modulate intracellular Ca^{2+} levels, slices were incubated for 1 h with the membrane-permeable Ca^{2+} chelator BAPTA-AM (dissolved in DMSO and diluted to a concentration of 50 μM in ACSF; final DMSO concentration 0.05%). To block both low- and high-voltage-activated Ca^{2+} channels, Ni^{2+} (100 μM) and Cd^{2+} (100 μM) were bath-applied. Glutamatergic AMPA and NMDA receptors were blocked with 50 μM 6-cyano-7-nitroquinoxaline-2,3-dione disodium (CNQX) and 100 μM of D(−)-2-amino-5-phosphonopentanoic acid. To assess the involvement of cAMP, slices were incubated for 30 min with 8-bromoadenosine 3′,5′-cyclic monophosphate (8-Br-cAMP, 500 μM) and 8-(4-chlorophenylthio) adenosine 3′,5′-cyclic monophosphate (500 μM). To block I_h channels, ZD7288 (50 μM) was bath-applied during whole-cell experiments and included in the pipette solution during cell-attached experiments. Chemicals were purchased from Sigma, Tocris, or Molecular Probes.

Dynamic Clamp. The functional consequences of changes in I_h at the soma were investigated in whole-cell current clamp recordings by using a dynamic clamp to artificially manipulate the amplitude of I_h. A personal computer with data acquisition card (National Instruments, Austin, TX) sampled membrane voltage at 5 kHz and injected I_h with the same sampling rate. The voltage dependence of I_h was taken from the fit to I_h from our experiments (with V in mV): $I_h(V) = I_{h\,max}/\{1 + \exp[(V + 141)/20.5]\}$. The amplitude ($I_{h\,max}$) was controlled by the external stimulus input of the HEKA amplifier. Rate constants $\alpha(V) = 0.071/\{1 + \exp[(V + 108)/8.3]\}$ and $\beta(V) = 0.24/\{1 + \exp[(V + 26.5)/-23]\}$ determined the time constants $\tau(V) = 1/\alpha(V) + \beta(V)$ for activation and deactivation. They were fit to the voltage range given in ref. 13 and, after correction for temperature and Na^+ concentration, matched to our own data set. To attain a fast and uniform response time of the real-time computer model, the functions were tabulated with the 12-bit input and output resolution of the hardware system. The properties of I_h in the dynamic clamp model were verified in voltage clamp mode.

Analysis. I_h recorded in the cell-attached configuration was leak corrected by using an online leak substraction protocol (P/4) in which leak pulses were determined from a relative holding potential of +20 mV to a range of relative membrane potentials between +22.5 and −20 mV. Current amplitude was determined as the mean value at 750–850 ms after the start of hyperpolarizing voltage steps. The time constant of activation of I_h was determined by fitting a single exponential function to the start of current traces. All values are given as mean ± SEM. Statistical differences were tested by nonparametric Mann–Whitney test or by Student's t test. $P < 0.05$ was used to indicate a significant difference.

Results

Characterization of I_h in the Somatic Compartment of CA1 Pyramidal Neurons. Hyperpolarization-activated currents were recorded in the whole-cell voltage clamp configuration from CA1 pyramidal neurons in hippocampal slices. Because of the high density of I_h channels in the distal dendrites of these neurons (13, 14, 16, 17), somatic I_h was isolated from the majority of dendritic I_h by cutting off the dendrites in the slices (see *Methods*). Step hyperpolarizations from a holding potential of −50 mV resulted in slowly activating inward currents (Fig. 1*A*), which were blocked in the presence of 50 μM ZD7288 (Fig. 1*A*). I_h was isolated by subtracting current traces before and after application of ZD7288 (Fig. 1*A*). The *I–V* curve of somatic I_h displayed inward rectification and a threshold of activation of around −60 mV (Fig. 1*B*). The activation curve for somatic I_h was generated by determining tail current amplitudes and fitting the normalized amplitudes with a Boltzmann equation (Fig. 1*B Inset*). The voltage-dependency of activation showed a voltage of half-maximal activation of −86 ± 2 mV and a slope parameter of 9.3 ± 0.9 mV ($n = 4$). Somatic I_h showed a typical slow activation time course (100–400 ms) that became faster with deeper hyperpolarization (Fig. 1*C*), and I_h did not inactivate over a period of 1,000 ms.

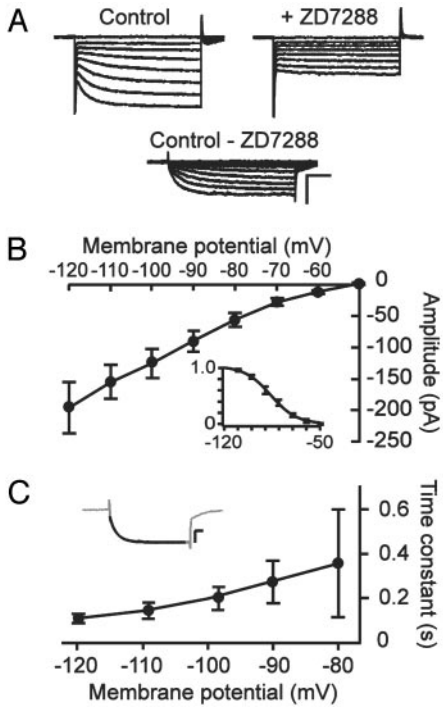

Fig. 1. Characterization of somatic I_h in CA1 pyramidal neurons. (*A*) Hyperpolarization-activated currents recorded in whole-cell mode with the majority of the dendrites cut off. Currents were evoked by stepping from a holding potential of −50 mV to membrane potentials ranging from −60 to −120 mV in 10 mV decrements. Bath application of 50 μM ZD7288 blocked slow hyperpolarization-activated currents, and I_h was isolated by subtracting current traces before and after addition of ZD7288. (Scale bars, 250 pA and 200 ms.) (*B*) *I–V* relationship of somatic I_h. (*Inset*) Boltzmann fit to the normalized current activation as a function of membrane potential generated from tail current amplitudes measured 20 ms after step repolarization. (*C*) Time constant of activation of I_h, as determined by fitting a single exponential function to the rising phase of current traces (*Inset*). (Scale bars, 100 pA and 100 ms.) Data represent mean ± SEM of four to five cells.

Enhanced Synaptic Activity Increases Somatic I_h. To study whether synaptic activity can modulate I_h, a nonselective increase in synaptic activity in intact slices was induced by bath application of 0.15 nM α-LTX in the presence of 1 μM tetrodotoxin. Because I_h is highly sensitive to modulation by intracellular components (11, 12), I_h was recorded from somatic cell-attached patches of CA1 pyramidal neurons. Hyperpolarizing voltage steps were

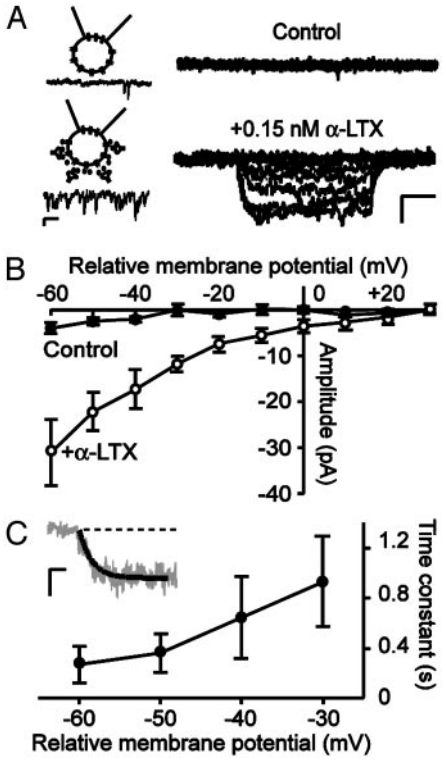

Fig. 2. Enhancement of synaptic activity by α-LTX induces an increase in somatic I_h. (*A*) I_h before (*Upper*) and after (*Lower*) bath application of 0.15 nM α-LTX for 15–25 min in the same cell. Currents were recorded from somatic cell-attached patches of CA1 pyramidal neurons with intact dendrites and were evoked by step hyperpolarizations from a relative membrane potential of +20 mV to potentials ranging from +30 to −60 in 10-mV decrements. (Scale bars, 25 pA and 250 ms.) Cartoons on the left are schematic representations of the recording configuration in the absence (*Upper*) and presence (*Lower*) of α-LTX. Below cartoons, example traces of miniature synaptic events recorded in a separate whole-cell experiment at a holding potential of −60 mV. (Scale bars, 5 pA and 200 ms.) (*B*) *I–V* curve of I_h before (filled symbols) and after (open symbols) bath application of α-LTX. (*C*) Activation kinetics of I_h. A single exponential function (solid line in inset) was fitted to the rising phase of I_h. (*Inset*) Example trace recorded at a relative membrane potential of −60 mV. (Scale bars, 20 pA and 100 ms.) Data points represent mean ± SEM of 6–10 cells.

applied from a relative membrane potential of +20 mV. Under control conditions, stepping to a relative membrane potential of −60 mV resulted in little inward current (4 ± 1 pA, Fig. 2*B*). Bath application of α-LTX for 15–25 min enhanced the synaptic activity in the slice throughout the duration of recordings (Fig. 2*A Inset*). In 10 of 13 somatic patches, the enhanced synaptic activity increased the amplitude of I_h at a relative membrane potential of −60 mV ≈8-fold to a mean value of 31 ± 7 pA ($P < 0.05$, compared with control). In the other three patches, no change in I_h amplitude was seen. The *I–V* curve of I_h in the presence of α-LTX displayed inward rectification and a threshold for activation at a relative membrane potential of ≈0 mV, which corresponds to the cell's resting membrane potential (Fig. 2*B*). Tail current amplitudes of cell-attached I_h were too small to accurately determine the voltage dependence of activation. The cell-attached I_h had a slow time course of activation (300–900 ms), which became faster with deeper hyperpolarization (Fig. 2*C*) and I_h showed no inactivation. These results demonstrate that a period of enhanced synaptic activity in the slice increases I_h on the soma of CA1 pyramidal neurons.

Enhanced Glutamatergic, but not GABAergic, Activity Increases Somatic I_h. Because the majority of synaptic terminals targeting CA1 pyramidal neurons are glutamatergic, we determined

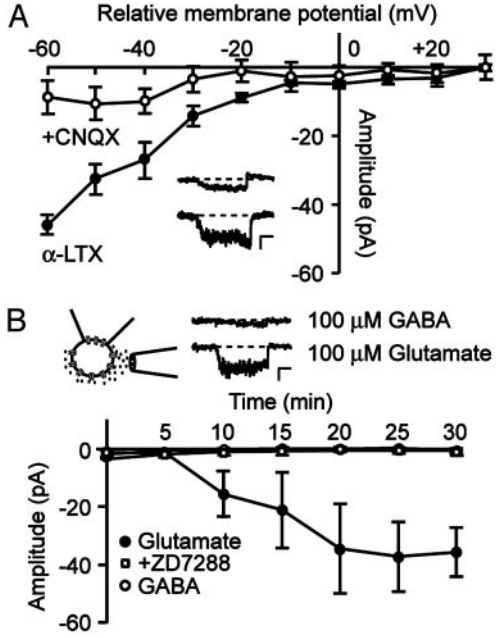

Fig. 3. Enhanced glutamatergic activity increases I_h. (*A*) *I–V* curve of cell-attached I_h recorded in the presence of 0.15 nM α-LTX (filled symbols) and after subsequent bath application of the AMPA receptor antagonist CNQX (50 μM, open symbols). (*Inset*) Current traces, recorded by stepping to a relative membrane potential of −60 mV in the presence of α-LTX (lower) and after addition of CNQX (upper). (Scale bars, 20 pA and 250 ms.) (*B*) Glutamate or GABA was applied near the soma by short and repeated pressure application. Pressure application of 100 μM glutamate (filled circles) gradually increased the amplitude of I_h, whereas application of 100 μM GABA (open circles) had no detectable effect. Including 50 μM ZD7288 (open squares) in the pipette solution prevented the increase in I_h. The cartoon is a schematic representation of the recording configuration. Example current traces are shown that were recorded by stepping to a relative membrane potential of −60 mV after glutamate (lower) and GABA (upper) application. (Scale bars, 10 pA and 250 ms.) Data points represent mean ± SEM of four to seven cells.

whether glutamate mediates the activity-induced increase in I_h. Bath application of the AMPA receptor antagonist CNQX (50 μM), subsequent to inducing the α-LTX effect on I_h, reversed the increase in I_h amplitude (Fig. 3*A*), suggesting a requirement for prolonged enhanced glutamatergic activity via AMPA receptors in the α-LTX-induced effect. Therefore, we studied whether direct pressure application of glutamate could mimic the effect of α-LTX on I_h. Glutamate (100 μM) was applied by using short and repetitive pressure application from a second pipette near the soma of the neuron under investigation. Within 10 min of application, in seven of nine patches, glutamate induced a gradual increase in I_h amplitude recorded at a relative membrane potential of −60 mV from 1 ± 1 pA to 36 ± 8 pA at 30 min after the start of glutamate application ($P < 0.05$ compared with control, Fig. 3*B*). In two patches, no change in I_h amplitude was seen. The gradual increase in I_h was prevented by including 50 μM ZD7288 in the pipette solution (1 ± 1 pA at $t = 30$, $n = 7$; Fig. 3*B*). Control recordings in which ACSF was pressure-applied did not show an increase in I_h (5 ± 4 pA at $t = 30$, $n = 5$; data not shown). Pressure application of the inhibitory neurotransmitter GABA (100 μM) had no detectable effect on I_h (1 ± 1 pA at $t = 30$, $n = 5$; Fig. 3*B*). This result suggests that up-regulation of I_h is specifically related to enhanced excitatory glutamatergic but not to inhibitory GABAergic activity, although decreases in I_h could escape detection.

AMPA-Receptor Mediated Depolarization and a Rise in Intracellular Ca^{2+} Concentration ($[Ca^{2+}]_i$) Are Required for the Increase in I_h. The underlying mechanism of the glutamate-induced increase in I_h

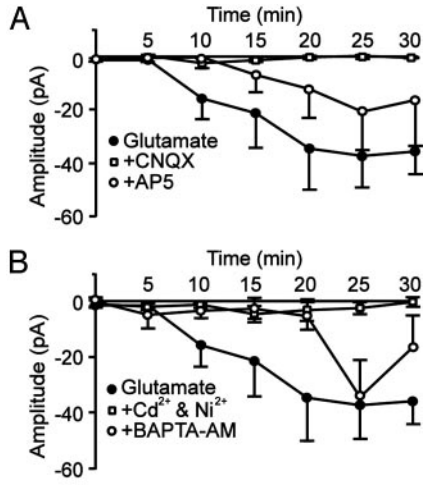

Fig. 4. AMPA receptor activation and a rise in $[Ca^{2+}]_i$ are required for the glutamate-induced increase in I_h. (*A*) Time course of the amplitude of I_h, recorded at a relative membrane potential of −60 mV during application of 100 μM glutamate (filled circles). In the continuous presence of 50 μM CNQX (open squares), the glutamate-induced increase in I_h was absent, whereas in the continuous presence of 100 μM D(−)-2-amino-5-phosphonopentanoic acid (AP5, open circles), the increase in I_h was reduced and its onset delayed. (*B*) The continuous presence of 100 μM Ni^{2+} and 100 μM Cd^{2+} (open squares) prevented the increase in I_h. The effect of glutamate on I_h was prevented for up to 20 min after the start of glutamate application by loading the cells with 50 μM BAPTA-AM to buffer intracellular Ca^{2+}(open circles). Data points represent mean ± SEM of four to seven cells.

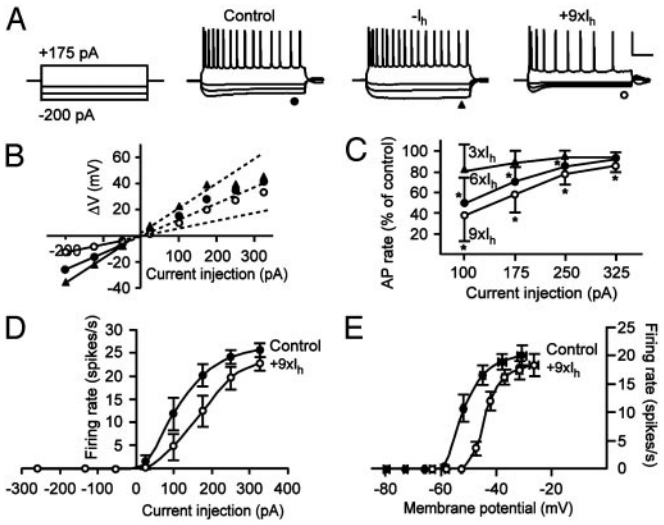

Fig. 5. Increased I_h reduces intrinsic excitability of CA1 pyramidal neurons. (*A*) Firing responses to a depolarizing (175 pA) current injection and hyperpolarizing (−50, −125, and −200 pA) current injections. Counteracting I_h by using a dynamic clamp abolished the depolarizing sag and tended to increase firing rate, whereas increasing I_h resulted in a more prominent sag and decreased firing rate. A dc was used to set the resting membrane potential at −60 mV. (Scale bars, 50 mV and 200 ms.) (*B*) Input resistance was calculated from the linear range (−200 to −50 pA) of *I–V* relationships determined at the end of voltage traces in control situation (filled circles), with counteracted I_h (triangles), and with increased I_h (open circles). (*C*) Firing rates in response to depolarizing current injections expressed as the percentage of control firing rates. Three different levels of I_h were used: 3× (triangles), 6× (filled circles), and 9× (open circles) the average somatic I_h as determined from separate whole-cell voltage clamp recordings (see Fig. 1). Asterisks indicate significant differences from control. (*D*) Firing rate as a function of depolarizing current injection for 9× I_h. Compared with control (filled symbols), the input–output relationship is shifted to the right with increased I_h (open symbols). (*E*) Firing rate as a function of the membrane potential in a separate set of experiments in which no dc was applied in control situation (closed symbols) and with increased I_h (open symbols). With increased I_h, the input–output relationship is shifted toward more depolarized potentials. Data points represent mean ± SEM of five to six cells.

was further investigated. In the continuous presence of 50 μM CNQX, the glutamate-induced increase in I_h amplitude was entirely prevented (Fig. 4*A*). In the presence of 100 μM D(−)-2-amino-5-phosphonopentanoic acid, the glutamate-induced increase in I_h was delayed and reduced in amplitude to ≈30–50% (Fig. 4*A*). These findings indicate that AMPA receptor activation alone can initiate the glutamate-induced increase in I_h, and that NMDA receptor activation has an additive effect.

Application of glutamate will depolarize the cell, a finding confirmed by separate whole-cell recordings showing that glutamate puffs induced a transient depolarization of 19 ± 3 mV (n = 4). To test whether direct depolarization also modulates I_h, we applied puffs of KCl (50 mM) near the soma of neurons, causing in whole-cell experiments a transient depolarization of 18 ± 3 mV (n = 4). In four of five cell-attached patches, puffs of KCl increased I_h with a similar time course as the glutamate puffs. The mean amplitude of I_h at a relative membrane potential of −60 mV after 30 min of KCl application was 120 ± 12 pA (n = 5; data not shown).

Because AMPA receptor-mediated depolarization and direct depolarization are likely to cause Ca^{2+} influx through voltage-gated Ca^{2+} channels, we studied the role of intracellular Ca^{2+} in the modulation of I_h. In the presence of Ni^{2+} (100 μM) and Cd^{2+} (100 μM), which block both low- and high-voltage-activated Ca^{2+} channels, glutamate application failed to induce an increase in I_h amplitude (Fig. 4*B*), suggesting that a rise in intracellular Ca^{2+} via voltage-gated Ca^{2+} channels is required for the modulation of I_h. This result was corroborated by the finding that buffering of $[Ca^{2+}]_i$ by incubating slices with the membrane-permeable analogue of the high affinity Ca^{2+} chelator BAPTA (50 μM) prevented the increase in I_h for up to 20 min after the start of glutamate application (Fig. 4*B*).

I_h channels are susceptible to modulation by cAMP (18–21). To investigate the involvement of cAMP in the increase in I_h, we incubated slices with the membrane-permeable analogues 8-bromoadenosine 3′,5′-cyclic monophosphate (8-Br-cAMP, 500 μM) and 8-(4-chlorophenylthio) adenosine 3′,5′-cyclic monophosphate (500 μM). After slices were incubated for 30 min with either 8-Br-cAMP or 8-(4-chlorophenylthio) adenosine 3′,5′-cyclic monophosphate, recordings from cell-attached patches showed a mean I_h amplitude at a relative membrane potential of −60 mV of 3 ± 1 pA (8-Br-cAMP, n = 8) and 2 ± 1 pA (8-(4-chlorophenylthio) adenosine 3′,5′-cyclic monophosphate; n = 3), which is not significantly different from control amplitudes, suggesting that an elevation of cAMP is not sufficient to induce an increase in cell-attached I_h and that the 8-fold increase in I_h, induced by glutamate is likely to be mediated by a cAMP-independent mechanism.

Increased I_h Reduces Intrinsic Excitability. Given the pivotal role of I_h in determining intrinsic excitability, we set out to determine the functional consequences of changes in somatic I_h on the firing behavior of CA1 pyramidal neurons. To effectively control the amplitude of I_h at the soma during whole-cell current clamp recordings, we used a dynamic clamp to artificially change I_h. Under control conditions, hyperpolarizing current injections evoked a hyperpolarization with a characteristic depolarizing sag reflecting the slow activation of I_h (Fig. 5*A*). In response to increasing depolarizing current injections, neurons fired with rates of up to 29 spikes per s. When the endogenous I_h was counteracted by the dynamic clamp, the depolarizing sag was obliterated, and firing rates tended to increase (Fig. 5*A*). Con-

versely, increasing I_h with the dynamic clamp resulted in a more pronounced depolarizing sag on hyperpolarization and strongly decreased firing rates in response to depolarizing current injections (Fig. 5*A*).

Changes in I_h will affect the input resistance of the neuron; therefore, the input resistance was determined from hyperpolarizing current injections (−200 to −50 pA) by using the slope of the *I–V* relationship in the linear range. Artificially counteracting the endogenous somatic I_h increased the input resistance from 100 ± 13 MΩ to 144 ± 28 MΩ ($n = 3$), whereas increasing I_h decreased the input resistance (Fig. 5*B*). The glutamate-induced increase in I_h found in the cell-attached recordings was ≈2–8 fold over the entire voltage range (Fig. 2*B*). Therefore, we increased the amplitude of I_h by a factor of 3, 6, or 9 times the mean I_h amplitude in the somatic compartment as recorded in separate whole-cell voltage clamp recordings (Fig. 1). In the control situation, the average input resistance was 102 ± 9 MΩ, which decreased to 74 ± 5 MΩ with 3× I_h, to 65 ± 3 MΩ with 6× I_h, and to 58 ± 2 MΩ with 9× I_h ($P < 0.05$, $n = 6$ in all cases).

The effect of increased I_h on firing rate was expressed as the percentage of control. Fig. 5*C* shows that increasing I_h six or nine times decreased firing rates over the entire range of current injections. The largest effect was found with the smallest current injections, indicating that I_h most strongly affects firing rates at membrane potentials that are relatively close to resting membrane potential. The relationship between firing rate and injected current, the input–output relationship, is shifted to the right as illustrated in Fig. 5*D* for the condition with 9× I_h. These results indicate that because of the reduced input resistance with increased I_h, a larger current injection is required to achieve a certain firing rate.

In all of these experiments, a DC current was injected to keep resting membrane potentials at −60 mV. However, under physiological conditions, increased I_h will also affect resting membrane potential and cause a small depolarization. A separate set of experiments was performed in which neurons were allowed to depolarize as a result of the increase of I_h. The depolarization amounted to 5 ± 1 mV for 3× I_h, 9 ± 1 mV for 6× I_h, and 12 ± 1 mV for 9× I_h ($P < 0.05$, $n = 5$ in all cases). Plotting the firing rate as a function of the voltage (the sum of the membrane potential and the depolarization induced over the decreased input resistance) showed that the dynamic range of the input–output relationship was shifted toward more depolarized potentials (Fig. 5*E*). Thus, the two parameters that are associated with an increase in I_h (a decreased input resistance and a depolarization) together shift the output range of CA1 pyramidal neurons in such a way that a higher level of excitation is required to reach a certain firing rate. The increase in I_h on enhanced excitatory synaptic activity can therefore serve as a homeostatic mechanism to control intrinsic excitability.

Discussion

Our experiments demonstrate that an enhancement of glutamatergic synaptic activity gradually increases the amplitude of I_h at the soma of hippocampal CA1 pyramidal neurons on a time scale of tens of minutes. This modulation depends on AMPA-receptor-mediated depolarization and on a rise of $[Ca^{2+}]_i$, and it appears to be cAMP-independent. Increasing I_h by using the dynamic clamp showed that increased I_h shifts the input–output relationship toward more depolarized potentials and that this mechanism can therefore serve as a homeostatic mechanism in response to enhanced excitatory synaptic activity. It has previously been shown that long-lasting changes in synaptic activity modulate voltage-gated conductances at a time scale of hours to days (4–8). Together with other recent studies (22–24), the results described here suggest that more rapid mechanisms of cellular plasticity also exist. To our knowledge, however, this is the first study that reports direct evidence for a homeostatic modulation of voltage-gated conductances on a relatively short-term time scale.

The effect of enhanced synaptic activity on I_h amplitude was specifically related to glutamatergic excitatory activity, whereas GABAergic inhibitory activity had no detectable effect on I_h amplitude (Fig. 3*B*). AMPA-receptor-mediated depolarization as well as direct depolarization by KCl increased I_h, and preventing a rise in $[Ca^{2+}]_i$ by blocking Ca^{2+} influx or by buffering $[Ca^{2+}]_i$ abolished or reduced the increase of I_h (Fig. 4*B*). Because AMPA receptors on CA1 pyramidal neurons have a low Ca^{2+} permeability (25), we hypothesize that AMPA receptor-mediated depolarization results in Ca^{2+} influx through NMDA receptors and voltage-gated Ca^{2+} channels. It therefore seems likely that depolarization-induced Ca^{2+} influx is the primary requirement for up-regulation of I_h. Because of technical limitations, it proved difficult to test the bidirectionality of this effect. However, once induced, the increase in I_h could be reversed by blockade of AMPA receptors (Fig. 4*A*), indicating that factors that directly or indirectly reduce intracellular Ca^{2+} could potentially decrease I_h.

A rise in $[Ca^{2+}]_i$ can trigger several intracellular messenger pathways. The relatively slow time-course of I_h modulation suggests that it is not Ca^{2+} itself but rather the activation of downstream intracellular pathways that leads to modulation of I_h. In line with this hypothesis, we could not reproduce the large effect of α-LTX or glutamate application on I_h in whole-cell recordings (increase in I_h amplitude of 9.4 ± 0.2%, $n = 6$; data not shown). The large increase in I_h could not be mimicked by elevating cAMP levels, suggesting a Ca^{2+}-dependent but cAMP-independent modulation. It therefore seems likely that the modulation of I_h requires the convergent action of several factors, including AMPA receptor-mediated depolarization, a rise in $[Ca^{2+}]_i$, and the activation of signaling pathways downstream of Ca^{2+}.

Although the previously reported studies on the modulation of intrinsic voltage-gated conductances after long-lasting changes in activity (4–8) may involve the synthesis and incorporation of new ion channels, the more rapid time course of the effects observed here suggests the modulation of existing ion channels or alternatively the insertion of spare ion channels into the membrane. In experiments using α-LTX, 3 of 13 patches did not show an increase in I_h amplitudes, and with glutamate application, 2 of 9 patches also did not show an increased I_h. Because of the cell-attached configuration, the sampling of currents is restricted to a relatively small fraction of the somatic membrane. Regional differences in either existing or inserted channel densities may therefore underlie the large variation found in the increase of I_h in somatic patches.

Irrespective of the precise mechanism underlying the modulation of somatic I_h, the results of this study suggest that this form of modulation may be a potent mechanism to regulate intrinsic excitability and therefore represents a mechanism of cellular plasticity that acts on a relatively short-term time scale. Several forms of cellular plasticity exist in addition to, and in cooperation with, synapse-specific forms of plasticity (1–3). Interestingly, synapse-specific mechanisms of plasticity commonly thought to underlie learning and memory, such as long-term potentiation and long-term depression, take place on a time scale similar to that of the effects described in this study and also involve the concurrent action of glutamate receptors and $[Ca^{2+}]_i$. Presynaptic I_h channels have been suggested to play an important role in several forms of long-term synaptic plasticity (refs. 26 and 27, but see ref. 28). Whether the modulation we describe here also affects presynaptic I_h channels remains to be determined.

I_h channels are present in much lower densities at the soma than at the dendrites of CA1 pyramidal neurons (13, 14, 16, 17). Dendritic I_h channels play an important functional role in determining the integrative properties of dendrites by dampen-

ing dendritic excitability and normalizing temporal summation (13, 14, 16). It is yet unknown whether dendritic I_h channels are also modulated in response to changes in synaptic activity or whether the mechanism we describe here is typically confined to the somatic compartment. In CA1 pyramidal neurons, the levels of I_h increase ≈7-fold from the soma toward the distal dendrites (13). If the mechanism we describe here is typically confined to the somatic compartment, it could function to locally regulate and control action potential generation. If the increase in I_h in response to excitatory synaptic activity is uniformly present in all neuronal compartments, it most likely serves as a general homeostatic cellular mechanism to dampen excitability and thus to scale the output of CA1 pyramidal neurons according to the level of excitatory input they receive.

We thank Sascha du Lac for discussions and comments on the manuscript, Marian Joëls and Fernando Lopes da Silva for their comments on an earlier version of the manuscript, and Oscar van den Bosch for writing the dynamic clamp model. J.A.v.H. is supported by a fellowship from the Royal Netherlands Academy of Arts and Sciences.

1. Marder, E., Abbott, L. F., Turrigiano, G. G., Liu, Z. & Golowasch, J. (1996) *Proc. Natl. Acad. Sci. USA* **93,** 13481–13486.
2. Turrigiano, G. G. (1999) *Trends Neurosci.* **22,** 221–227.
3. Burrone, J., O'Byrne, M. & Murthy, V. N. (2002) *Nature* **420,** 414–418.
4. Turrigiano, G. G., LeMasson, G. & Marder, E. (1995) *J. Neurosci.* **15,** 3640–3652.
5. Desai, N. S., Rutherford, L. C. & Turrigiano, G. G. (1999) *Nat. Neurosci.* **2,** 515–520.
6. Baines, R. A., Uhler, J. P., Thompson, A., Sweeney, S. T. & Bate, M. (2001) *J. Neurosci.* **21,** 1523–1531.
7. Golowasch, J., Abbot, L. F. & Marder, E. (1999) *J. Neurosci.* **19,** RC33.
8. Aizenman, C. D., Akerman, C. J., Jensen, K. R. & Cline, H. T. (2003) *Neuron* **39,** 831–842.
9. Hille, B. (2001) *Ion Channels of Excitable Membranes* (Sinauer, Sunderland, MA).
10. Macaferri, G., Mangoni, M., Lazzari, A. & DiFrancesco, D. (1993) *J. Neurophysiol.* **69,** 2129–2136.
11. Pape, H. C. (1996) *Annu. Rev. Physiol.* **58,** 299–327.
12. Robinson, R. B. & Siegelbaum, S. A. (2002) *Annu. Rev. Physiol.* **65,** 29.1–29.28.
13. Magee, J. C. (1998) *J. Neurosci.* **18,** 7613–7624.
14. Magee, J. C. (1999) *Nat. Neurosci.* **2,** 508–514.
15. Capogna, M., Gahwiler, B. H. & Thompson, S. M. (1996) *J. Neurophysiol.* **76,** 3149–3158.
16. Poolos, N. P., Migliore, M. & Johnston, D. (2002) *Nat. Neurosci.* **5,** 767–774.
17. Lorinz, A., Notomi, T., Tamas, G., Shigemoto, R. & Nusser, Z. (2002) *Nat. Neurosci.* **5,** 1185–1193.
18. McCormick, D. A. & Pape, H. C. (1990) *J. Physiol. (London)* **431,** 319–342.
19. Ingram, S. L. & Williams, J. T. (1996) *J. Physiol. (London)* **492,** 97–106.
20. Luthi, A. & McCormick, D. A. (1999) *Nat. Neurosci.* **2,** 634–641.
21. Pedarzani, P. & Storm, J. F. (1995) *Proc. Natl. Acad. Sci. USA* **92,** 11716–11720.
22. Aizenman, C. D. & Linden, D. J. (2000) *Nat. Neurosci.* **3,** 109–111.
23. Egorov, A. V., Hamam, B. N., Fransen, E., Hasselmo, M. E. & Alonso A. A. (2002) *Nature* **420,** 173–178.
24. Nelson, A. B., Krispel, C. M., Sekirnjak, C. & du Lac, S. (2003) *Neuron* **40,** 609–620.
25. Burnashev, N., Monyer, H., Seeburg, P. H. & Sakmann, B. (1992) *Neuron* **8,** 189–198.
26. Beaumont, V., Zhong, N., Froemke, R. C., Ball, R. W. & Zucker, R. S. (2002) *Neuron* **33,** 601–613.
27. Mellor, J., Nicoll, R. A. & Schmitz, D. (2002) *Science* **295,** 143–147.
28. Chevaleyre, V. & Castillo, P. E. (2002) *Proc. Natl. Acad. Sci. USA* **99,** 9538–9543.